

Outward Migration of a Gas Accreting Planet: A Semi-Analytical Formula

SHIGERU IDA (井田茂)^{1,2}, YA-PING LI (李亚平)³, JUN-PENG PAN (潘俊鹏)^{3,4}, YI-XIAN CHEN (陈逸贤)⁵, AND DOUGLAS N. C., LIN (林潮)^{6,2,7}

¹*Earth-Life Science Institute, Institute of Science Tokyo, Tokyo 152-8550, Japan*

²*Department of Astronomy, School of Science, Westlake University, Hangzhou, Zhejiang 310030, China*

³*Shanghai Astronomical Observatory, Chinese Academy of Sciences, Shanghai 200030, China*

⁴*University of Chinese Academy of Sciences, Beijing 100049, China*

⁵*Department of Astrophysics, Princeton University, Princeton, NJ 08544, USA*

⁶*Department of Astronomy & Astrophysics, University of California, Santa Cruz, CA 95064, USA*

⁷*Institute for Advanced Study, Tsinghua University, Beijing, 100084, China*

ABSTRACT

Type II orbital migration is a key process to regulate the mass and semimajor axis distribution of exoplanetary giant planets. The conventional formula of type II migration generally predicts too rapid inward migration to reconcile with the observed pile-up of gas giant beyond 1 au. Analyzing the recent high-resolution hydrodynamical simulations by Li et al. (2024) and Pan et al. (2025) that show robust outward migration of a gas accreting planet, we here clarify the condition for the outward migration to occur and derive a general semi-analytical formula that can be applied for broad range of planet mass and disk conditions. The striking outward migration is caused by azimuthal asymmetry in corotation torque exerted from circumplanetary disk regions (connecting to horseshoe flow) that is produced by the planetary gas accretion, while the conventional inward migration model is based on radial asymmetry in the torques from the circumstellar protoplanetary disk. We found that the azimuthal asymmetry dominates and the migration is outward, when the gap depth defined by the surface density reduction factor of $1/(1 + K')$ is in the range of $0.03 \lesssim K' \lesssim 50$. Using simple models with the new formula, we demonstrate that the outward migration plays an important role in shaping the mass and semimajor axis distribution of gas giants. The concurrent dependence of planets' accretion rate and migration direction on their masses and disk properties potentially reproduces the observed pile-up of exoplanetary gas giants beyond 1 au, although more detailed planet population synthesis calculations are needed in the future.

Keywords: Accretion(14), Protoplanetary disks(1300), Extrasolar gaseous giant planets(509)

1. INTRODUCTION

Gas giants with masses $\gtrsim 0.3 \times$ Jupiter mass, which were discovered by radial velocity (RV) surveys, show a clear pile-up at the semimajor axes $a \gtrsim 1$ au. The occurrence rate of these gas giants jumps up by a factor of more than 3-5 at 1 au and it is almost constant up to ~ 5 au. (e.g., Wittenmyer et al. 2020). The orbital period bias of RV observations for gas giants would be very weak for $\lesssim 5$ au, and the possible bias tends to restrict detection in large a planets. Therefore, the pile-up at $a \gtrsim 1$ au must be real.

Several papers addressed possible origins of the pile-up. High-resolution hydrodynamical simulations found that type II migration of a gas giant is not tied to disk accretion (Duffell et al. 2014; Kanagawa et al. 2015b; Dürmann & Kley 2017), in contrast to the pioneering

studies on gap-opening process (e.g., Lin & Papaloizou 1986; Lin et al. 1996). Accordingly, Kanagawa et al. (2018) proposed that type II migration is no other than type I migration with lower disk surface density in the bottom of a gap - the migration of a high-mass gas giant is slowed down simply by the fraction of surrounding gas it depletes. However, the slowing-down due only to the nominal gap formation is not enough to account for the pile-up. This is because type I migration is fast and a very deep gap is created only after the planet mass exceeds a Jupiter mass (e.g., Ida et al. 2018, see Section 3.4).

Type II migration could be further slowed down by additional depletion in the disk surface density by disk wind (Ida et al. 2018), photoevaporation (Tanaka et al. 2020), or a steep surface density profile (Chen et al.

2020). In particular, the global disk gas depletion caused by gas accretion onto the planet (Tanigawa & Tanaka 2016) is very important, which is discussed in detail in Section 3.4. Another idea is that planetesimals are initially concentrated in the regions beyond the snow line (e.g., Guo et al. 2025).

Migration process itself should also be investigated with high-resolution hydrodynamical simulations with planetary gas accretion. A forming gas giant planet concurrently accretes gas and migrates. Because the accretion modifies the gas surface density in the proximity of the planet, gas accretion must be taken into account in migration simulations.

Recently, robust outward migration for a Jupiter-mass planet concurrently accreting gas in the disk with the viscosity parameter $\alpha \gtrsim 3 \times 10^{-3}$ was reported by Li et al. (2024) with high-resolution 3D/2D hydrodynamical simulations. They found that this gas loss process results in steady azimuthal asymmetry in the circumplanetary disk (CPD) and horseshoe flows between leading and trailing regions and the asymmetry causes outward migration of the planet. Laune et al. (2024) also found through a few 2D hydrodynamical simulations, a disk-embedded companion around a host with mass ratio $q = 10^{-3}$ and $\alpha = 0.1$ undergoes outward migration if the companion efficiently accretes gas in the accretion disk. Their result is consistent with Li et al. (2024), although they did not explore the dependence on the disk viscosity.

We note that previous hydrodynamical simulations including the effect of the planetary gas accretion did not find outward migration (Dürmann & Kley 2015, 2017; Robert et al. 2018). Li et al. (2024) argued that the outward migration appears as a result of their self-consistent treatments of the planetary accretion and the outer boundary condition to ensure steady accretion of the protoplanetary disk (for boundary conditions, also see Dempsey et al. (2020) and Laune et al. (2024)), as well as high enough resolution for the CPD.

Pan et al. (2025) performed parameter surveys with high-resolution hydrodynamical simulations similar to Li et al. (2024). They changed planet-to-star mass ratio q , the viscosity parameter α , and disk aspect ratio h to make clear the parameter ranges for the outward migration. They found that the relevant parameter range is very wide, as shown in Section 3. These results should impact the arguments on migration of gas giants and the observed pile-up of exoplanetary gas giants at $a \gtrsim 1$ au.

In this paper, using the results by Pan et al. (2025), we derive semi-analytical formula for the migration rate as a function of q , α , and h to show intrinsic physics and the conditions for the outward migration clearly

and provide a useful tool for planet population synthesis calculations. We show that the effects of the azimuthal asymmetry due to planetary accretion on orbital migration (its direction and magnitude) relative to the conventional formula neglecting the azimuthal asymmetry are simply described only by the gap depth parameter (Kanagawa et al. 2015b).

For the planetary gas accretion rate, we combine the results of Tanigawa & Tanaka (2016), Choksi et al. (2023), and Li et al. (2023) to derive a relevant formula. The thermodynamics (radiation, equation of state) would play a critical role in the accretion rate onto the planet (Ayliffe & Bate 2009; Lambrechts et al. 2019; Lega et al. 2024) and in migration of accreting Jupiter-mass planets (Wu & Li 2024). However, the relevant thermodynamics is not clear yet. Here, in order to highlight the outward migration by the azimuthal asymmetry created by the planetary gas accretion, we leave the thermodynamic effects for future study. Wafflard-Fernandez & Lesur (2025) found outward migration in a giant planet in eccentric orbit in the disk-wind driven accretion disk. Significant eccentricity could be excited by planet-disk interaction in the case of high-mass giants (also see Dempsey et al. 2021). This effect will be commented in this paper, but the details are also left for future studies.

In Section 2, we summarize the past results of gap depth created by a planet and gas accretion rate onto the planet. Using these formulas and Pan et al. (2025)'s numerical results, in Section 3, we derive the outward migration condition and the general migration rate formula of a gas-accreting planet including both outward and inward migrations.

2. METHOD

2.1. Gap depth

As a gas giant grows, its gravitational perturbation generates a wide and smooth gap. The reduction factor of the surface density at the bottom of the gap (Σ_{gap}) relative to the unperturbed one outside the gap (Σ_0) is given by (Kanagawa et al. 2015b; Dempsey et al. 2020)

$$\frac{\Sigma_{\text{gap}}}{\Sigma_0} \simeq (1 + K')^{-1} \equiv f_{\text{gap}}, \quad (1)$$

where ¹

$$K' = 0.04 q^2 h^{-5} \alpha^{-1} = q_{\text{th}} q_{\text{vis}}; \quad (2)$$

$$q_{\text{th}} = q/h^3 = 8 \left(\frac{h}{0.05} \right)^{-3} \left(\frac{q}{10^{-3}} \right); \quad (3)$$

$$q_{\text{vis}} = 0.04 q_{\text{th}} h/\alpha = 16 \left(\frac{h}{0.05} \right)^{-2} \left(\frac{q}{10^{-3}} \right) \left(\frac{\alpha}{10^{-3}} \right)^{-1}; \quad (4)$$

$$q = \frac{m_{\text{p}}}{M_*}; \quad h = \frac{H}{r}, \quad (5)$$

where m_{p} and M_* are the planet and host star's masses, H is the disk gas scale height and α is the alpha parameter of the turbulent strength. The conventional thermal condition (the dominance of planetary perturbations over pressure gradient) and viscous gap formation condition are $q_{\text{th}} = 3(r_{\text{H}}/H)^3 \gtrsim 3$ and $q_{\text{vis}} = 0.04 q h^{-2} \alpha^{-1} \gtrsim 1.6$, respectively ².

2.2. The ability of gas accretion onto a giant planet

Tanigawa & Tanaka (2016) semi-analytically predicted the rate of gas accretion onto planet as a function of m_{p} . Rosenthal et al. (2020), Choksi et al. (2023) and Li et al. (2023) revisited this issue by performing high-resolution hydrodynamical simulations.

Choksi et al. (2023) and Li et al. (2023) performed 2D/3D global simulations with a sink corresponding to planetary gas accretion. The gas accretion is dominated by Bondi accretion for low-mass planets and by Hill accretion for high-mass planets. The switching mass is $q_{\text{th}} \sim 1$, because

$$\frac{R_{\text{B}}}{H} = \frac{G m_{\text{p}}}{H c_s^2} = q_{\text{th}} \quad (6)$$

$$\frac{R_{\text{H}}}{H} = \left(\frac{q}{3} \right)^{1/3} \frac{r}{H} = 3^{-1/3} q_{\text{th}}^{1/3}. \quad (7)$$

where R_{B} and R_{H} are Bondi and Hill radii, and we used $c_s^2 = H^2 \Omega^2 = G M_* h^2 / r$.

If $R_{\text{B}} \lesssim R_{\text{H}}$, equivalently $q_{\text{th}} \lesssim \sqrt{3}/3$, the planet has an envelope rather than a circumplanetary disk. In this case, $R_{\text{B}} \lesssim H$ and the gas accretion onto the planet would be described by Bondi accretion:

$$\dot{m}_{\text{B}} \simeq \pi R_{\text{B}}^2 \rho_{\text{gap}} c_s = \pi q_{\text{th}}^2 \rho_{\text{gap}} H^3 \Omega. \quad (8)$$

Both Choksi et al. (2023) and Li et al. (2023) found the q_{th}^2 dependence. Li et al. (2023) found a numerical factor several times smaller than π in the above and Choksi

et al. (2023) found a larger factor. Because they aimed to derive the q_{th} scaling, their inner boundary condition was simple and not consistent with steady accretion with reduction due to the planetary gas accretion (Fig. 2 shown later). Adopting a consistent boundary condition, Li et al. (2024) and Pan et al. (2025) obtained a numerical factor consistent with π , as well as confirmation of the q_{th}^2 dependence. Hence, we use Eq. (8). For convenience, we use Σ_{gap} rather than ρ_{gap} with a simple relation $\Sigma_{\text{gap}} = \sqrt{2\pi} \rho_{\text{gap}} H$ as

$$\dot{m}_{\text{B}} = \sqrt{\pi/2} q_{\text{th}}^2 \Sigma_{\text{gap}} H^2 \Omega. \quad (9)$$

When $R_{\text{H}} \gtrsim H$, equivalently $q_{\text{th}} \gtrsim 3$ the gas flow for planetary accretion can be approximated by 2D flow and is supplied by Kepler shear. In this case,

$$\begin{aligned} \dot{m}_{\text{H}} &\simeq 2R_{\text{H}} \times \frac{3}{2} R_{\text{H}} \Omega \times \Sigma_{\text{gap}} \\ &= 3 \left(\frac{q_{\text{th}}}{3} \right)^{2/3} \Sigma_{\text{gap}} H^2 \Omega. \end{aligned} \quad (10)$$

All of Choksi et al. (2023), Li et al. (2023), and Pan et al. (2025) found the $q_{\text{th}}^{2/3}$ dependence. However, the fitted numerical factor has uncertainty within a factor of 10 for super-Jupiter planets. Li et al. (2023) and Choksi et al. (2023) found a twice larger factor and a similar factor, respectively. Pan et al. (2025) obtained a several times larger factor. Although Pan et al. (2025) (and Li et al. (2024)) used the inner boundary condition consistent with the steady accretion, they may have had some difficulty in the case of high-mass planet with a very deep gap. Therefore, in this paper, we use a simple formula given by Eq. (10) for Hill accretion. We will discuss the effect of the uncertainty in the numerical factor in Section 3.4.

In the above, there is a transition regime between the Bondi and the Hill accretion regime $\sqrt{3}/3 \gtrsim q_{\text{th}} \gtrsim 3$. We adopt smooth connection between the two regions as Eq. (13), without discussing the transition regime.

We will use the above Li et al. (2023); Choksi et al. (2023) type accretion rate. On the other hand, we also compare them with Tanigawa & Tanaka (2016)'s formula with in Section 2.3.

With the same notations, Tanigawa & Tanaka (2016) derived the semi-analytical formula based on the fitting of 2D local simulations without a sink by Tanigawa & Watanabe (2002) as

$$\dot{m}_{\text{BH}} \simeq 0.29 q_{\text{th}}^{4/3} \Sigma_{\text{gap}} H^2 \Omega, \quad (11)$$

which we refer as ‘‘TT’’ formula. Although they did not consider Bondi accretion regime, the dependence $\dot{m}_{\text{BH}} \propto$

¹ We define $K' = 0.04K$ here to distinguish the parameter K usually defined in the literature, where $K = q^2 h^{-5} \alpha^{-1}$.

² Lin & Papaloizou (1986) derived the viscous condition as $q \gtrsim 40\nu/r\Omega \simeq 40\alpha h^2 = 1/(0.025 h^{-2} \alpha^{-1})$.

$q_{\text{th}}^{4/3}$ of their formula is in between the Bondi ($\propto q_{\text{th}}^2$) and Hill ($\propto q_{\text{th}}^{2/3}$) scalings. As shown below, their formula gives approximation of the Li/Choksi scaling³.

Assuming the steady accretion, the unperturbed disk gas accretion is

$$\dot{m}_{\text{d}} \simeq 3\pi\Sigma_0\nu = 3\pi\alpha\Sigma_0H^2\Omega. \quad (12)$$

The combined *local* Bondi and Hill accretion scaled by \dot{m}_{d} is given by

$$\frac{\dot{m}_{\text{p,loc}}}{\dot{m}_{\text{d}}} = \frac{1}{(1+K')} \left(\frac{\dot{m}_{\text{B}}}{\dot{m}_{\text{d}}} + \frac{\dot{m}_{\text{H}}}{\dot{m}_{\text{d}}} \right)^{-1}, \quad (13)$$

$$\frac{\dot{m}_{\text{B}}}{\dot{m}_{\text{d}}} = \frac{\sqrt{\pi/2}}{3\pi} q_{\text{th}}^2 \alpha^{-1}; \quad \frac{\dot{m}_{\text{H}}}{\dot{m}_{\text{d}}} = \frac{3^{1/3}}{3\pi} q_{\text{th}}^{2/3} \alpha^{-1} \quad (14)$$

and Tanigawa & Tanaka (2016)'s (TT) formula is

$$\frac{\dot{m}_{\text{p,loc}}}{\dot{m}_{\text{d}}} = \frac{1}{(1+K')} \times \frac{0.29}{3\pi} q_{\text{th}}^{4/3} \alpha^{-1}, \quad (15)$$

where the subscript “loc” means the *local* expressions of the planetary gas accretion that does not consider a limit by global disk gas flow and it can exceed \dot{m}_{d} .

2.3. Actual rates of planetary gas accretion and gas flow across the planetary orbit

With $\dot{m}_{\text{p,loc}}$ larger than the disk accretion rate \dot{m}_{d} , the actual efficiency of gas accretion onto a planet, taking account of feedback from the limited supply, is derived as (Tanigawa & Tanaka 2016; Rosenthal et al. 2020)

$$f_{\text{p}} = \frac{\dot{m}_{\text{p}}}{\dot{m}_{\text{d}}} = \frac{\xi}{(1+\xi)}; \quad \xi = \frac{\dot{m}_{\text{p,loc}}}{\dot{m}_{\text{d}}}, \quad (16)$$

such that when $\xi \gg 1$ (the ability of gas accretion by the planet is large enough), this equation shows that most of gas flowing through the disk is accreted onto the planet ($f_{\text{p}} = \dot{m}_{\text{p}}/\dot{m}_{\text{d}} \sim 1$).

Figure 1a show $\dot{m}_{\text{p,loc}}/\dot{m}_{\text{d}} = \xi$ for the Li/Choksi and TT formulas by red and blue lines, respectively. From Eqs. (13) and (14),

$$\xi = \frac{1}{3\pi\alpha(1+K')} \left(\sqrt{2/\pi} q_{\text{th}}^{-2} + 3^{-1/3} q_{\text{th}}^{-2/3} \right)^{-1}. \quad (17)$$

In the limits of $q_{\text{th}} \gg 1$ ($K' = 0.04q_{\text{th}}^2 h/\alpha \gg 1$),

$$\xi \simeq 1.2 \times 10^2 K'^{-2/3} h_{0.05}^{-1/3} \alpha_3^{-2/3}, \quad (18)$$

³ The 4/3 scaling is also observed in a series of local 3D simulations (Maeda et al. 2022, 2024), though the reasons for its discrepancy with global simulations is unclear.

where

$$h_{0.05} = h/0.05; \quad \alpha_3 = \alpha/10^{-3}. \quad (19)$$

In this case, the gap is so deep that the accretion onto the planet is limited.

For $q_{\text{th}} \ll 1$ ($K' \ll 1$),

$$\xi \simeq (3\pi\sqrt{2/\pi}\alpha)^{-1} q_{\text{th}}^2 \simeq 66 h_{0.05}^{-1} K'. \quad (20)$$

In this limit, the planet gravity is not strong enough to capture most of the disk gas accretion. In both limits, $\xi \ll 1$ ($\dot{m}_{\text{p,loc}} \ll \dot{m}_{\text{d}}$). The effect of the planetary gas accretion is pronounced ($\xi > 1$) for modest values of q_{th} .

Figure 1b shows the actual planetary accretion efficiency, $f_{\text{p}} = \dot{m}_{\text{p}}/\dot{m}_{\text{d}} = \xi/(1+\xi)$, with the Li/Choksi and TT formulas. The region with $\dot{m}_{\text{p}} \sim \dot{m}_{\text{d}}$ (full planetary accretion) expands around $q_{\text{th}} \sim 1$.

Since the fraction of disk gas accretion that accretes onto the planet is $f_{\text{p}} = \xi/(1+\xi)$, the rest of accretion will pass through the planet's orbit, leading to a reduced disk gas accretion flux and correspondingly, to the reduced surface density Σ_0 in the inner disk with a factor of

$$f_{\text{pass}} = \frac{1}{1+\xi}. \quad (21)$$

In both limits of $q_{\text{th}} \gg 1$ and $q_{\text{th}} \ll 1$, $\xi \ll 1$ and $f_{\text{pass}} \simeq 1$. For modest values of q_{th} , f_{pass} can be significantly smaller than a unity, as shown in Figure 1c. The maximum reduction in both paradigms can reach a factor of 10-50 ($f_{\text{pass}} \sim 0.02 - 0.1$).

We note that this approximation introduces a puzzle for massive planets in the limit of $q_{\text{th}} \gg 1$ and $\xi \ll 1$. It is reasonable that $\xi \ll 1$ means $f_{\text{p}} \ll 1$, because planetary accretion is quenched by a deepest gap. But, the deepest gap should also prevent gas flow through the planetary orbit, which is inconsistent with $f_{\text{pass}} \simeq 1$. We will discuss this issue in Section 4.

2.4. Global reduction in disk gas surface density due to planetary gas accretion

The gas surface density with the effect of planetary gas accretion under the steady accretion is analytically derived by Tanigawa & Tanaka (2016):

$$\Sigma_0 = (1 - f_{\text{p}}) \left(1 - \sqrt{\frac{r_{\text{in}}}{r}} \right) \frac{\dot{m}_{\text{d}}}{3\pi\nu} \quad [r_{\text{in}} < r < r_{\text{p}}], \quad (22)$$

$$\Sigma_0 = \left[(1 - f_{\text{p}}) \left(1 - \sqrt{\frac{r_{\text{in}}}{r}} \right) + f_{\text{p}} \left(1 - \sqrt{\frac{r_{\text{p}}}{r}} \right) \right] \times \frac{\dot{m}_{\text{d}}}{3\pi\nu} \quad [r > r_{\text{p}}], \quad (23)$$

where r_{in} and r_{p} are the radii of the disk inner edge and the planet's orbit, respectively, and $\nu = \alpha h^2 r^2 \Omega$. Radial

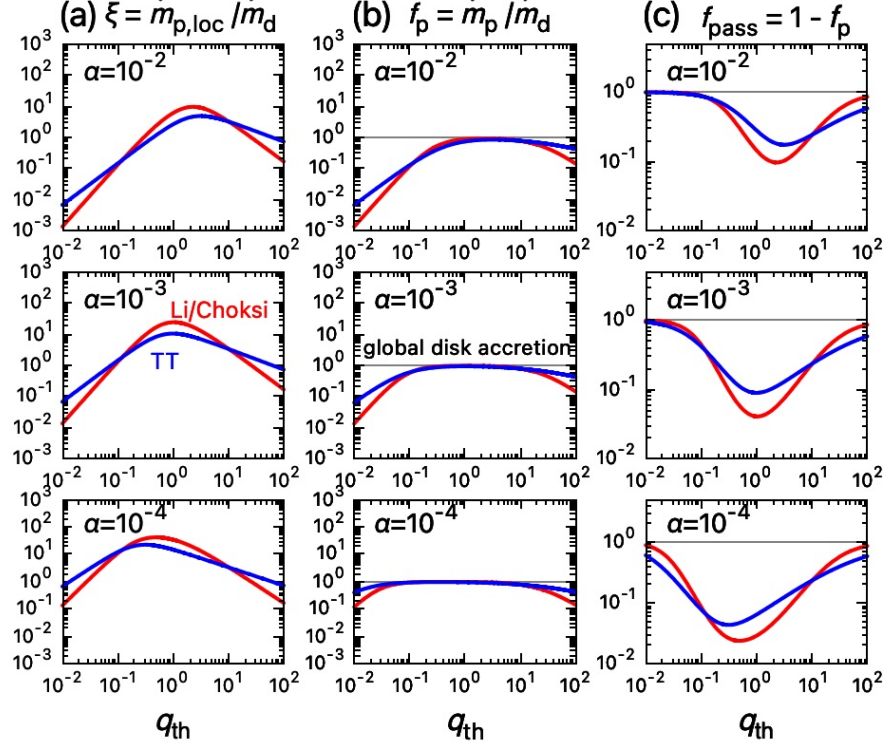


Figure 1. The efficiency of gas accretion onto planet as a function of q_{th} , predicted by Li/Choksi (red lines) and TT (blue lines) formulas. In panels (a), the ability of planetary gas accretion ($\xi = \dot{m}_{\text{p,loc}}/\dot{m}_{\text{d}}$) are plotted. The dependence on α is shown in the upper, middle and lower panels, with a fixed value of $h = 0.05$. In panels (b), the actual ability with a cap of the disk accretion ($f_{\text{p}} = \dot{m}_{\text{p}}/\dot{m}_{\text{d}}$) is shown. The panels (c) show the corresponding reduction $f_{\text{pass}} (= 1 - f_{\text{p}})$ in the global gas surface density.

profile of Σ_0 is plotted in Fig. 2 for $\xi = 2$ ($f_{\text{p}} = 2/3$) and $\xi = 10$ ($f_{\text{p}} = 0.91$).

This analytical formula for Σ_0 distribution with a planet sink was reproduced by 3D global hydrodynamical simulation (Figure D2 in Li et al. (2023)). Thus, the unperturbed (no gap) disk density at $r \simeq r_{\text{p}}$ is reduced by a factor of $(1 - f_{\text{p}})$ from that at large distance to the planet's orbit.

The actual surface density is further reduced by gap opening from this value of Σ_0 . In the remainder of this paper, for more direct comparison with the results from Li et al. (2024) and Pan et al. (2025), we adopt the accretion rate scalings in Eqs. (13) and (14) in calculating the planet accretion rate f_{p} .

If f_{p} is large enough, say $\xi \gtrsim 2$, the planetary accretion effect in the disk global depletion is significant (see Fig. 2). The condition $\xi \gtrsim \xi_{\text{acc}} = 2$ reads as (Eq. (20) with $q_{\text{th}} \ll 1$)

$$K' \gtrsim K'_{\text{acc}} \equiv 0.03 h_{0.05} \left(\frac{\xi_{\text{acc}}}{2} \right). \quad (24)$$

With $K' = 128 h_{0.05}^{-5} (q/10^{-3})^2 \alpha_3^{-1}$ (Eq. (2)), Eq. (24) is

$$q \gtrsim 1.5 \times 10^{-5} h_{0.05}^3 \alpha_3^{1/2} \left(\frac{\xi_{\text{acc}}}{2} \right)^{1/2}. \quad (25)$$

We point out that even a super-earth inside a very shallow gap ($0.03 \lesssim K' \ll 1$) accretes most of disk gas flow through it. However, Eq. (17) assumes that the planet has already bypassed the Kelvin-Helmholtz contraction limit and is undergoing runaway gas accretion. Equivalently, m_{p} must be larger than the critical core mass $\sim 10 M_{\oplus}$ ($q \sim 3 \times 10^{-5}$).

2.5. Conventional type-I and type-II migration rates

The conventional type-I migration rate is given by Tanaka et al. (2002)

$$\frac{\dot{a}_{\text{I}}}{a} \sim -q \frac{\pi \Sigma_0 r_{\text{p}}^2}{M_*} h^{-2} \Omega, \quad (26)$$

where Σ_0 is an unperturbed local surface density of disk gas. In this paper, we assume the planet orbit is circular and the orbital radius r_{p} is equal to the semimajor axis a of the planet. Here, we define *outward* migration rate with a plus sign and *inward* disk accretion rate

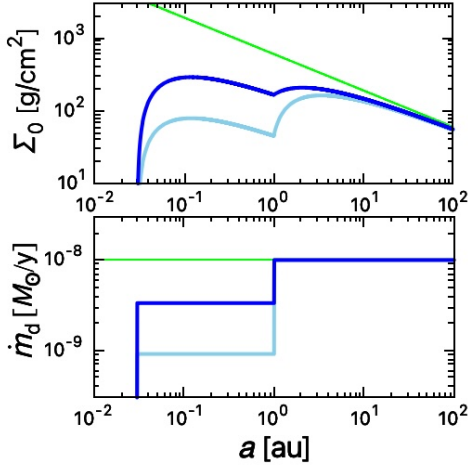


Figure 2. The Σ_0 distribution (the upper panel) and gas accretion rate through the disk (the lower panel) in the steady state with the effect of gas accretion onto the planet and host star (sinks) is plotted in the case of $\dot{m}_d = 10^{-8} M_\odot/\text{yr}$, $\alpha = 10^{-3}$, $h = 0.05$, $r_{\text{in}} = 0.03 \text{ au}$, and $r_p = 1 \text{ au}$. The green, blue, and skyblue lines are the distribution without any sink, and those with the planet sinks with $\xi = 2$ ($f_p = 2/3$) and $\xi = 10$ ($f_p = 0.91$), respectively. For $\alpha = 10^{-3}$ and $h = 0.05$, $\xi = 2$ corresponds to $q = 1.6 \times 10^{-5}$ and $q = 1.86 \times 10^{-3}$, and $\xi = 10$ corresponds to $q = 4.2 \times 10^{-5}$ and $q = 4.9 \times 10^{-4}$. With the sinks, \dot{m}_d decreases by the accretion onto the planet inside 1 au and vanishes by the accretion onto the host star at r_{in} .

\dot{m}_d is defined with a plus sign, in order to make clear the planet migration direction. Using the steady disk accretion rate $\dot{m}_d = 3\pi \Sigma_0 \alpha h^2 r^2 \Omega$, Eq. (26) is

$$\frac{\dot{a}_I}{a} \sim -\frac{q}{3\alpha h^4} \frac{\dot{m}_d}{M_*} \simeq -4.7 \times 10^3 K'^{1/2} \alpha_3^{-1/2} h_{0.05}^{-3/2} \frac{\dot{m}_d}{M_*}. \quad (27)$$

where we used $q = 5\sqrt{K'h^5\alpha}$ (Eq. 2). Because the effect of gas accretion onto a planet on migration is regulated by K' , as shown below, we use type I migration formula as a function of K' rather than q .

According to Kanagawa et al. (2018), type II migration rate is fitted by

$$\frac{\dot{a}_{\text{II,gap}}}{a} \simeq \frac{1}{1 + K'} \frac{\dot{a}_I}{a}, \quad (28)$$

which we will refer to as the “type II (gap)” formula. Tanigawa & Tanaka (2016) and Tanaka et al. (2020) proposed the further reduction of type II migration rate caused by the global gas surface density depletion due to gas accretion onto a planet (Fig. 2). For a modest value of q_{th} (~ 1), the global surface density reduction significantly slows down migration as well as the local surface density reduction by gap opening. Accordingly,

the type II migration rate is modified to be

$$\frac{\dot{a}_{\text{II,gap+dep}}}{a} \sim \frac{f_{\text{pass}}}{(1 + K')} \frac{\dot{a}_I}{a}, \quad (29)$$

which we will refer to as the “type II (gap+dep)” formula.

Because K' and f_{pass} (equivalently, ξ) are functions of only α , h and q , the theoretical migration rates scaled by \dot{m}_d/M_* are also functions of only α , h and q , independent of Σ_0 , as long as steady accretion is established.

3. RESULTS

3.1. Summary of hydrodynamical simulations

We first summarize the high-resolution hydrodynamical simulations by Li et al. (2024) and Pan et al. (2025). They showed that gradual mass loss from the disk gas in horseshoe orbits to the planet through a circumplanetary disk (CPD) during encounters in many horseshoe excursions starting in the leading side, results in slightly higher gas surface density in the leading CPD region than in the trailing region. Here we define “CPD” as the dense region rotating around the planet in prograde direction that is connected to horseshoe flow. In an Eulerian view, the steadily higher surface density in leading side always accelerates the planet orbital motion, resulting in positive net angular momentum transfer from the disk to the planet. In other words, corotation torque that is azimuthally asymmetric between the leading and trailing sides of the planet changes migration speed and even direction in some parameter range.

Pan et al. (2025) performed systematic surveys of simulations to show how the migration rate depends on the simulation parameters, α , q , and h . The upper panels of Figure 3 summarize their surveys (square symbols) and show that migration is outward ($\dot{a}/a > 0$) in wide ranges of parameters.

Li et al. (2024) already found that outward migration of a Jupiter-mass planet ($q = 10^{-3}$) changes to inward migration for $\alpha \lesssim 3 \times 10^{-3}$, which is shown in panel (a). In panel (b), for a fixed value of α ($= 10^{-3}$), the q dependence is shown. Outward migration is found in lower q region. These two figures suggest that outward migration is not favored in too deep gap cases ($K' \propto q^2 \alpha^{-1} h^{-5}$).

Panel (c) shows the q dependence with higher α ($= 0.04$) than that in Panel (b). The outward migration region expands to higher q region here. In Panel (d), while $\alpha = 0.04$ is the same as Panel (c), smaller h ($= 0.03$) is used. The outward migration region shifts lower q region than in Panel (c). These two figures strongly support the above idea of gap depth.

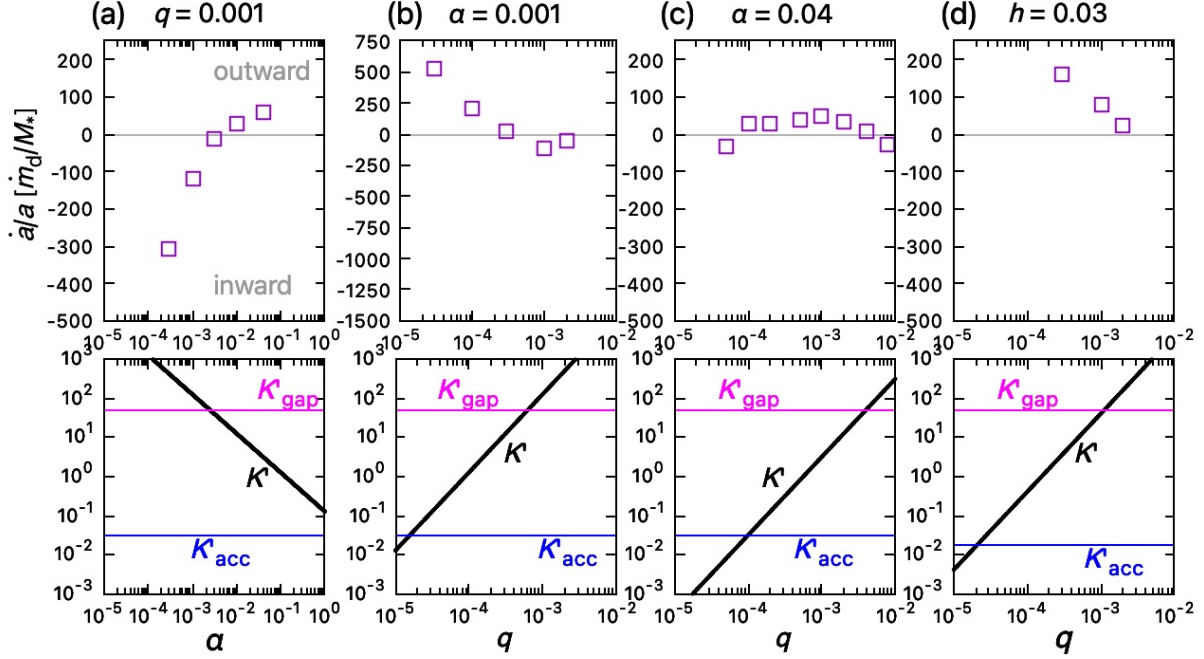


Figure 3. The migration rates obtained by Pan et al. (2025) and Li et al. (2024) (upper panels). The scaling factor is \dot{m}_d/M_* , where \dot{m}_d is the disk mass accretion rate and M_* is the host star mass. The simulation parameters are the planet to star mass ratio $q = m_p/M_*$, the disk viscosity parameter α , and the disk aspect ratio $h = H/r$. Except for panel (d), $h = 0.05$ is used. In panel (d), $\alpha = 0.04$. The vertical scales are different in panel (b) for visual convenience. In each of the lower panels, K' corresponds to the parameters in the directly upper panel. The outward migration is predicted in $K'_{\text{acc}} < K' < K'_{\text{gap}}$ for $\xi_{\text{acc}} = 2$ ($K'_{\text{acc}} = 0.03$) and $K'_{\text{gap}} = 50$.

On the other hand, Panel (c) shows that there is also a lower limit in gap depth for outward migration to occur. Based on these hydrodynamical simulation survey results, we next derive the condition for outward migration.

3.2. Outward migration conditions

Analyzing the summarized simulation results in upper panels of Fig. 3 in details, we find that the migration is outward, if the gap is not too deep to maintain the dominance of horseshoe corotation torque over Lindblad torque (detailed discussion is given in Section 3.3) and if the planet accretes most of disk gas flow to retain the azimuthal horseshoe asymmetry. Therefore, the gap-depth parameter K' [$\Sigma_{\text{gap}}/\Sigma_0 = 1/(1 + K')$] is the most important parameter for the occurrence of the outward migration.

In the lower panels of Fig. 3, we plot K' analytically determined from α, h and q in each of the parameter surveys as $K' = 0.04 q_{\text{th}}^2 h \alpha^{-1} = 2 h_{0.05} \alpha_3^{-1} q_{\text{th}}^2$ where $q_{\text{th}} = 8 h_{0.05}^{-3} (q/10^{-3})$.

We find that the outward migration regime corresponds to similar range of K' in all the panels (all of the parameter surveys). The dependence on either of

α, h and q is reduced to that on the single parameter K' .

The upper limit of K' for the outward migration is found as

$$K' \sim K'_{\text{gap}} = 50. \quad (30)$$

Li et al. (2024) found that outward migration of a planet with $q = 10^{-3}$ is turned to inward migration for $\alpha \lesssim 3 \times 10^{-3}$ (Fig. 3a). Below this critical α value, the gap is so deep that the horseshoe corotation torque no longer dominates the Lindblad torque, and the gas accretion onto the planet, which makes the azimuthal asymmetry, is quenched.

On the other hand, the lower limit of K' for the outward migration is $K'_{\text{acc}} \sim 0.03$, as shown in Fig. 3. From Eq. (20) for $q_{\text{th}} \ll 1$, the upper limit of ξ (> 1) for the outward migration is

$$\xi_{\text{acc}} \simeq 2 h_{0.05}^{-1} \left(\frac{K'_{\text{acc}}}{0.03} \right). \quad (31)$$

The fraction of accretion onto a planet in upstream gas accretion through the disk is given by $\xi/(1 + \xi)$, which is $2/3$ for $\xi = 2$. If more than two thirds of disk gas accretes onto a planet, the resultant azimuthally asymmetric torque reverses the migration direction. For the

parameters, $q = 10^{-3}$, $\alpha = 0.1$, and $h = 0.07$, where [Laune et al. \(2024\)](#) found outward migration, $K' \simeq 0.24$, which is also within the above outward migration range.

Thus, the condition for outward migration is simply given by $K'_{\text{acc}} \lesssim K' \lesssim K'_{\text{gap}}$, or more explicitly by

$$0.03 h_{0.05} \left(\frac{\xi_{\text{acc}}}{2} \right) \lesssim K' \lesssim 50 \left(\frac{K'_{\text{gap}}}{50} \right). \quad (32)$$

The parameters K'_{gap} ($\gg 1$) and ξ_{acc} (> 1) should be empirically determined by comparison with the hydrodynamical simulation results, such as $K'_{\text{gap}} \sim 50$ and $\xi_{\text{acc}} \sim 2$. The range of outward migration, $0.03 \lesssim K' \lesssim 50$, is broad enough to impact planet formation models. In the case of $\alpha = 10^{-3}$ and $h = 0.05$, the outward migration range is as broad as $q = 1.5 \times 10^{-5}$ to $q = 6.3 \times 10^{-4}$ (from super-earths to 2 Saturn's mass gas giants). We note that q must be larger than the critical core, $q \sim 3 \times 10^{-5}$, to initiate the runaway gas accretion and generate the asymmetry by the accretion onto the planet. It is safer to set the lower limit at $q \sim 3 \times 10^{-5}$.

Because the outward migration condition is determined solely by K' , we can easily derive a (semi-) analytical formula of migration rate including outward migration as in Section 3.3.

The semi-analytical formula including the azimuthal asymmetry in addition to the effects of the gap opening and the global depletion will be referred to as “type II (full)” formula.

3.3. General semi-analytical formula for orbital migration rates including both outward and inward migrations

The results of [Pan et al. \(2025\)](#)'s simulations are compared with the existing type II (gap) and type II (gap+dep) formulas in Fig. 4. It shows that

$$\frac{\dot{a}}{a} \simeq - \left(\frac{\dot{a}}{a} \right)_{\text{gap+dep}} [K'_{\text{acc}} \lesssim K' \lesssim K'_{\text{gap}}], \quad (33)$$

where $K'_{\text{acc}} \sim 0.03$ and $K'_{\text{gap}} \sim 50$. Because $(\dot{a}/a)_{\text{gap+dep}}$ in Eq. (33) is negative (inward), the fitting rate, \dot{a}/a , is positive (outward). The type II (gap+dep) formula is given by Eq. (29) with Eq. (27):

$$\left(\frac{\dot{a}_{\text{II}}}{a} \right)_{\text{gap+dep}} \simeq \frac{1}{(1 + K')} \frac{1}{(1 + \xi)} \frac{\dot{a}_{\text{I}}}{a}, \quad (34)$$

where \dot{a}_{I}/a is given by Eq. (27)

$$\frac{\dot{a}_{\text{I}}}{a} \simeq -4.7 \times 10^3 K'^{1/2} \alpha_3^{-1/2} h_{0.05}^{-3/2} \frac{\dot{m}_{\text{d}}}{M_*}, \quad (35)$$

and ξ is given as a function of K' , α and h by Eq. (17) with Eqs. (2) and (3).

A possible interpretation of Eq. (33) is as follows. [Tanaka & Okada \(2024\)](#) analytically derived 3D Lindblad and corotation torques due to radial asymmetries in the protoplanetary disks: the torque components due to curvature, the radial gradients of $\Sigma_0 \propto r^{-\zeta}$, $P \propto r^{-\delta}$, $H \propto r^{\mu}$, and $T \propto r^{-\chi}$. Assuming steady disk gas accretion $\mu = -\chi/2 + 3/2$ ($3\pi\Sigma_0\nu = 3\pi\Sigma_0\alpha H^2\Omega$ is constant of r), ideal gas $\delta = \zeta + \mu + \chi$ ($P \propto \rho T \propto \Sigma_0 T/H$), and that the local gas surface density is uniform, they derived the Lindblad and corotation torques as

$$\Gamma_{\text{L}}/\Gamma_0 = -(2.382 + 0.094\zeta + 1.297\chi) \quad (36)$$

$$\Gamma_{\text{c}}/\Gamma_0 = 0.946 - 0.630\zeta + 0.858\chi, \quad (37)$$

where $\Gamma_0 = q^2 h^{-2} \Sigma_0 r^4 \Omega^2$. In the no gap cases, the total torque⁴ $\Gamma = \Gamma_{\text{L}} + \Gamma_{\text{c}} = -(1.436 + 0.724\zeta + 0.439\chi) \Gamma_0$ is always negative (inward migration) for $\zeta, \chi > 0$. Both Γ_{L} and Γ_{c} are included in the calculation of \dot{a}_{I} .

In the gap opened cases, Σ locally (in radial scale $\ll r$) changes. Because the gap half width is relatively large (Eq. (41)), Lindblad resonances, which are broadly distributed in the gap bottom regions, are significantly weakened. On the other hand, a CPD is formed when a gap is opened. Because the scale height of the CPD is smaller than that of the circumstellar (protoplanetary) disk ([Li et al. 2023](#)), the density is higher in the CPD. Accordingly, corotation torque exerted from the horseshoe flows connected to the CPD dominates Lindblad torque and $\Gamma \sim \Gamma_{\text{c}}$, in the case of a modest gap.

Furthermore, the azimuthal asymmetry enhances Γ_{c} . As we already described, the disk gas repeats many encounters during many horseshoe excursions, gradually losing mass to the planet, until it completely passes the planet orbit. Because the mass loss starts in the leading horseshoe region, slightly higher gas surface density is established in the leading horseshoe region than in the trailing region and this azimuthal asymmetry causes outward migration. [Pan et al. \(2025\)](#) (see also [Li et al. \(2024\)](#)) shows that the migration is outward at $q_{\text{th}} \sim O(1)$ if the planetary accretion is included, while it is still inward otherwise (the leading and trailing flows are symmetric).

The degree of the azimuthal asymmetry is estimated as follows. As discussed in Section 2.2, the rate of planetary gas accretion is self-regulated to be equal to \dot{m}_{d} when outward migration occurs. The gas in horseshoe excursions would drifts inward on average by the disk global viscous diffusion. The timescale for the mean disk gas flow to cross the gap by the radial drift velocity

⁴ For $\zeta = 0.5$ and $\chi = 1$ that [Pan et al. \(2025\)](#) adopted, $\dot{a}/a = 2\Gamma \simeq -4.5\Gamma_0$, which is consistent with Eq. (26).

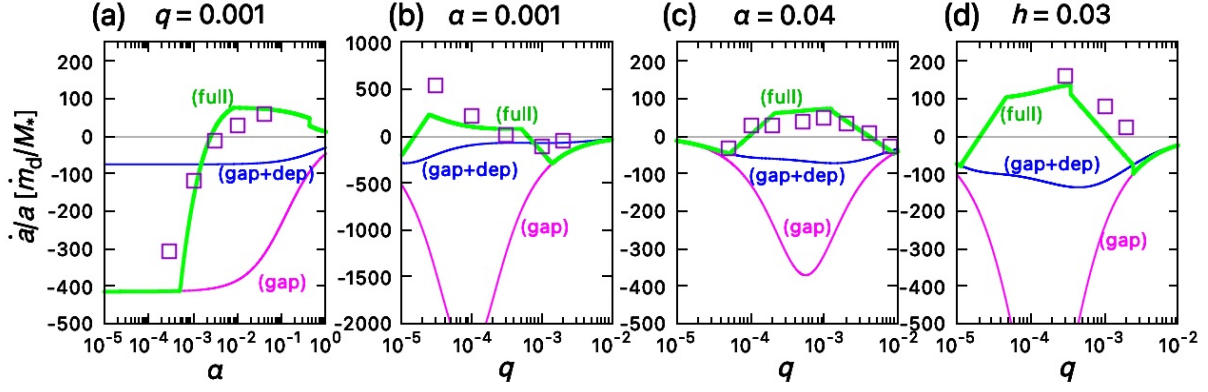


Figure 4. The general semi-analytical migration formula [type II (full) formula] including the azimuthal asymmetry in addition to the effects of the gap opening and the global depletion due to the planetary gas accretion (green lines). It is compared with the type II (gap) formula with only the gap opening effect (magenta lines), the type II (gap+dep) formula with the gap opening and the global depletion effects (blue lines), and four systematic parameters survey results of hydrodynamical simulations by Pan et al. (2025) (brown squares), which are the same panels as in the upper panels in Fig. 3.

due to the diffusion ($v_r \simeq -(3/2)\nu/r$) is

$$t_{\text{cross}} \sim \frac{2\Delta_{\text{gap}}}{3\alpha H^2 \Omega / 2r} = \frac{4(\Delta_{\text{gap}}/r)}{3\alpha h^2 \Omega}, \quad (38)$$

where Δ_{gap} is the gap half-width. The excursion timescale of a horseshoe orbit is

$$t_{\text{hs}} \sim \frac{2\pi r}{(3/2)\Delta_{\text{gap}}\Omega} = \frac{4\pi}{3(\Delta_{\text{gap}}/r)\Omega}. \quad (39)$$

Because the horseshoe flow loses almost all of the mass in t_{cross} , the averaged decrease in Σ due to the planetary gas accretion during one horseshoe encounter is $\Delta\Sigma \sim \Sigma/N$, where $N \sim t_{\text{cross}}/t_{\text{hs}}$. Consequently, the azimuthal asymmetry between the leading and trailing horseshoe regions would be

$$\frac{\Delta\Sigma}{\Sigma} \sim \frac{t_{\text{hs}}}{t_{\text{cross}}} \sim \pi \frac{\alpha h^2}{(\Delta_{\text{gap}}/r)^2}. \quad (40)$$

Kanagawa et al. (2015a) derived an empirical formula for Δ_{gap} by the definition of $\Sigma = \Sigma_0/2$. Because we are concerned with the edge of the gap bottom, we use a half value of their Δ_{gap} as

$$\frac{\Delta_{\text{gap}}}{r} = \frac{1}{2} \times \left[0.41 \left(\frac{K' h^2}{0.04} \right)^{1/4} \right]. \quad (41)$$

Substituting this equation into Eq. (40), we obtain

$$\frac{\Delta\Sigma}{\Sigma} \sim \frac{(4/5)\pi}{0.41^2} K'^2 \alpha h \sim 1.5 \left(\frac{K'}{10} \right)^2 \alpha_3 h. \quad (42)$$

Therefore, the azimuthal torque asymmetry would be $\sim h$, and it is comparable to the radial torque asymmetry (e.g., Miyoshi et al. 1999; Kley & Nelson 2012).

This explains why the absolute value of outward migration rate due to the azimuthal asymmetry is comparable (at least by the order of unity) to that of type II (gap+dep) inward migration rate due to the radial asymmetry (Eq. 33).

In order to use Eq. (33) for planet population synthesis, we need to derive the fitting formula including the transition regimes between the outward and ordinary inward migration regimes at least continuously (we do not require smoothness). Here we apply a log-linear interpolation of K' on the $\dot{a}/a - q$ or $\dot{a}/a - \alpha$ plots in Fig. 4. We define detaching points as the linear interpolation meets type II (gap+dep) formula in these plots. We empirically find that the hydrodynamical simulation results in Fig. 4 meet the interpolation at the higher parameter $K' \sim K'_{\text{gap,h}} = 5 K'_{\text{gap}} = 250$ and at the lower one $K' \sim K'_{\text{acc,l}} 10^{-1/2} = K'_{\text{acc}} = 0.01 h_{0.05}$. We log-linearly connect the fitting migration rate given by Eq. (33) to $(\dot{a}/a)_{\text{gap+dep}}$ with the condition of $\dot{a}/a = 0$ at K'_{gap} and K'_{acc} and the detaching points at $K'_{\text{gap,h}}$ and $K'_{\text{acc,l}}$ as

$$\frac{\dot{a}}{a} \simeq \left(\frac{\dot{a}}{a} \right)_{\text{gap+dep,l}} \left(\frac{\log K'_{\text{acc}} - \log K'}{\log K'_{\text{acc}} - \log K'_{\text{acc,l}}} \right) \quad (43)$$

$$[K'_{\text{acc,l}} < K' \lesssim K'_{\text{acc}}]$$

$$\frac{\dot{a}}{a} \simeq \left(\frac{\dot{a}}{a} \right)_{\text{gap,h}} \left(\frac{\log K' - \log K'_{\text{gap}}}{\log K'_{\text{gap,h}} - \log K'_{\text{gap}}} \right) \quad (44)$$

$$[K'_{\text{gap}} \lesssim K' < K'_{\text{gap,h}}],$$

where $(\dot{a}/a)_{\text{gap+dep,l}}$ and $(\dot{a}/a)_{\text{gap,h}}$ are $(\dot{a}/a)_{\text{gap+dep}}$ at $K' = K'_{\text{acc,l}}$ and $(\dot{a}/a)_{\text{gap}}$ at $K' = K'_{\text{gap,h}}$. As Fig. 3a clearly shows, simulation results converge to “type II (gap)” rather than “type II (gap+dep)” in high K' regimes, because the gap is so deep there that the global

disk depletion effect may be no longer applicable. This formula (type II (full)) is plotted in Fig. 4 by green lines. The formula consistently reproduces the Pan et al. (2025)’s results within a factor of 2 in broad ranges of parameters.

3.4. Concurrent growth and migration of gaseous planets

In order to demonstrate the impact of the outward migration on planet formation, we concurrently integrate the planetary growth by gas accretion,

$$\frac{\dot{m}_p}{m_p} = \frac{\xi}{(1 + \xi)} \frac{\dot{m}_d}{m_p} \quad (45)$$

and its migration with type II (full) formula in Section 3.3. For planetary gas accretion, we also include the early phase of Kelvin-Helmholtz contraction limit into account (Ida et al. 2018).

Assuming the self-similar solution of a viscously expanding disk (Lynden-Bell & Pringle 1974) where $T = 130 (r/1 \text{ au})^{-1/2} \text{ K}$ and $\dot{m}_d = 3 \times 10^{-8} (1 + t/t_{\text{diff}})^{-3/2} M_\odot/\text{yr}$ with $t_{\text{diff}} = 10^6 \text{ yrs}$, the mass and semimajor axis evolution of independent planets are shown in Fig. 5. We start integration from $10 M_\oplus$ planets in 3 – 30 au. The interactions between planets are neglected in this particular calculations to highlight the outward migration, avoiding complex dynamics, although planetary interactions (resonance trapping, scattering, and collisions) were included in our previous population synthesis calculations (Ida & Lin 2010; Ida et al. 2013, 2018).

Figure 5a shows comparison of results among type II (gap), (gap+dep), and (full) formulas. According to the hydrodynamical simulation results, we adopt type II (gap) formula at $K' > K'_{\text{gap}}$ even in the calculation marked by type II (gap+dep).

Comparison between type II (gap) and (gap+dep) formulas show that the effect of the global disk depletion due to the planetary gas accretion significantly reduces inward migration of gas giants (also see Tanaka et al. 2020). It also shows that the outward migration due to planetary gas accretion brings planets further in particular in the outer region. In the outermost region, the outward migration rather brings planets formed in $\gtrsim 20 \text{ au}$ to the outermost regions of the disk ($\gtrsim 300 \text{ au}$).

Figures 5b and c show runaway gas accretion and outward migration simultaneously occur around a few $\times 10^5 \text{ yrs}$ integration from $10 M_\oplus$ cores. During this phase, almost all the disk gas flow accretes onto the planet.

In Fig. 5c, the evolution paths of K' in individual planets are plotted. Because $K' \propto q^2 h^{-5}$ and $h \propto r^{1/4}$ in this calculation, K' of each planet in inner regions is already high at $10 M_\oplus$ and quickly increases as the planet

growth to overshoot the outward migration regime of $K'_{\text{acc}} < K' < K'_{\text{gap}}$, and the migration turns into inward one.

On the other hand, in outer regions, K' is initially smaller and it is within the outward migration regime even if the planet acquires a Jupiter mass. Therefore, the outward migration impacts planets in outer regions and it would significantly contribute to retain gas giants beyond 1 au. This also means that the runaway gas accretion lasts longer in outer regions (see panels a and b) and planets there can acquire larger final masses.

The planets starting at 18 and 30 au keep outward migration to reach the disk outermost regions of 300 au. In this case, the increase in the planetary mass is compensated by the increase in r and h , so that the increase in K' is slower and the outward migration tends to be preserved. If we set the radially exponential decay in the surface density in the self-similarity solution, the outward migration would stop at the decaying region.

Because this is converging migration, if planet-planet interactions are included, shepherding or strong scattering would happen. It could potentially form HR8799-like systems, where multiple gas giants exist in almost circular orbits at $\sim 15\text{--}70 \text{ au}$, while the giant planets around 1 au could also be formed in the same systems. However, we note that the existence of planets that keep outward migration depends on disk conditions and actual gas accretion rates.

As pointed out in Section 2.2, hydrodynamical simulation results still have uncertainty in numerical factors of planetary gas accretion rate. Pan et al. (2025) suggests that the theoretical estimate in Eq. (10) may underestimate the accretion rate in Hill regime. Figure 5d shows the result with 10 times enhancement in the accretion rate in Hill regime in type II (full) formula, as an extreme case, to be compared with the result with the fiducial type II (full) formula. Because the growth is accelerated, K' tends to quickly escape from the outward migration regime and the planets that keep outward migration disappear. They disappear even with 3 times enhancement in the Hill accretion rate and also with that in the initial \dot{m}_d .

Nevertheless, Figure 5e shows that the mass-semimajor axis evolution is hardly affected by the factor 10 enhancement in the Hill accretion rate, except for the outermost planets. This is because the planetary accretion rate has a cap by \dot{m}_d . Thus, the uncertainty in a factor of planetary gas accretion rate does not significantly affect the results in this paper.

Finally, we point out that if some mechanism enhances accretion onto the planet in the deep gap (Section 4), the final planet distribution should be shifted further

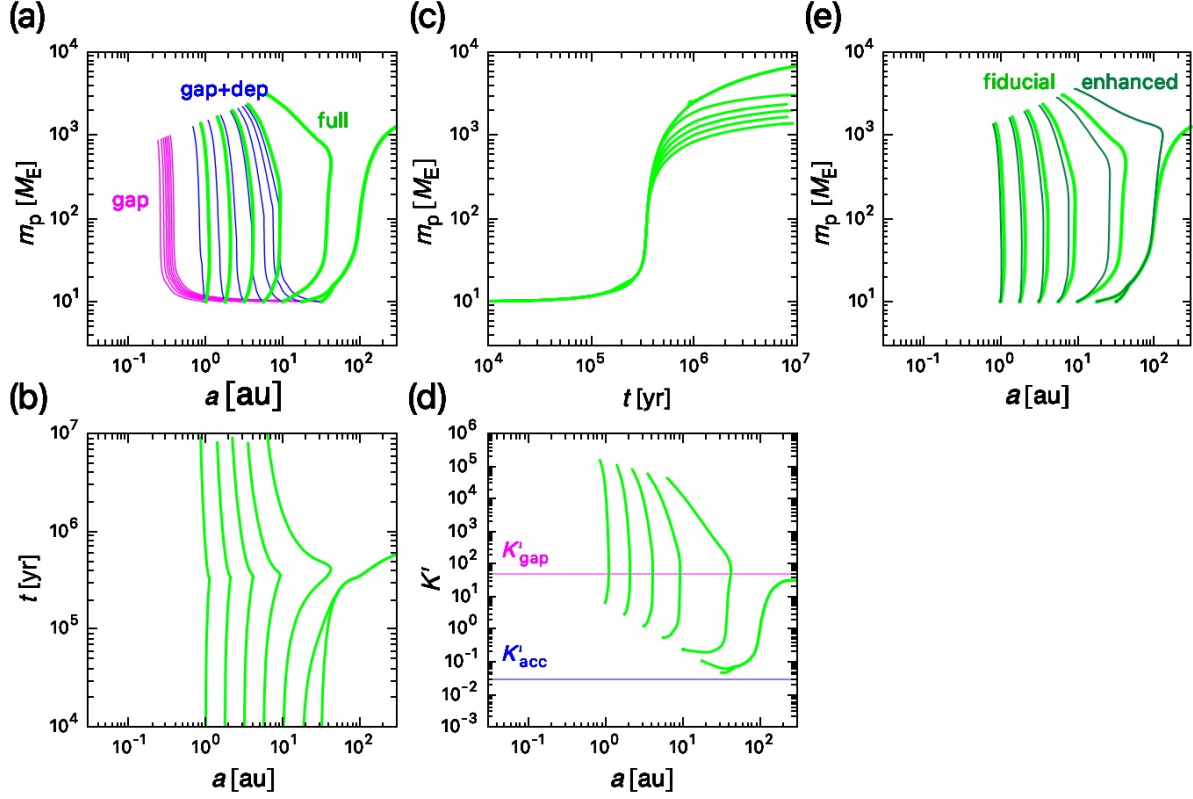


Figure 5. The mass and semimajor axis evolution of independent planets starting from $m_p = 10M_\oplus$ at 9 different locations of $a = 1 - 30$ au (Panel (a)). For the disk, the self-similar solution with $\dot{m}_d = 3 \times 10^{-8} (1 + t/t_{\text{diff}})^{-3/2} M_\odot/\text{yr}$ with $t_{\text{diff}} = 10^6$ yrs and $T = 130 (r/1 \text{ au})^{-1/2} \text{K}$ is used. The evolution with type II (full) formula in Section 3.3 is shown in the green lines. For comparison, the evolutions with type II (gap) and type II (gap+dep) formulas are also shown in the magenta and blue lines. The evolution is integrated until $t = 10^7$ yrs. In Panels (b), (c), and (d), time evolution of the semimajor axis, the mass, and the gap parameter (K') of individual planets are shown with type II (full) formula. In Panel (e), the result with enhanced Hill accretion rate by a factor 10 in type II (full) formula (dark green) is compared to the fiducial result (green).

outward, compared with that predicted by the type II (gap+dep) formula.

4. DISCUSSION

In Li et al. (2024) and Pan et al. (2025), r_p is fixed. They estimated the migration from the torques from the Σ distribution influenced by the planetary accretion. Following their method, in this paper, we have approximated that $f_{\text{pass}} + f_p \simeq 1$.

As Fig. 1 shows, when a planet grows and q_{th} exceeds ~ 10 , a gap becomes so deep that f_p decreases as q_{th} increases. With the assumption of $f_{\text{pass}} + f_p \simeq 1$, in this case, f_{pass} must increase toward $\simeq 1$. However, the very deep gap should also prevent disk gas from crossing the gap, and it may be more appropriate that $f_{\text{pass}} + f_p \ll 1$.

This inconsistency can only be resolved by either planetary migration or the breakdown of steady flow with mass accumulation (beyond r_p) until the resumption of diffusion through the gap. The mass accretion and the

migration affect each other in a complicated manner (for detailed discussion, see Pan et al. 2025).

Chen et al. (2020) suggested that in the deep gap cases, $f_{\text{pass}} \ll 1$ and disk gas piles up outside the planetary orbit to push the planet inward, although they neglected the effect of planetary gas accretion. On the other hand, Pan et al. (2025) suggest the eccentricity of the disk excited by the planet or other factors enhance accretion onto the planet in the deep gap cases. More detailed analysis on the deep gap cases is left to the future study.

5. CONCLUSION

To understand the observed mass and semimajor axis distribution of exoplanetary giant planets, type II orbital migration is a key process.

Following Li et al. (2024)'s discovery of outward migration of a Jupiter-mass planet that accretes gas from the disk, Pan et al. (2025) performed parameter surveys

to clearly show the broad parameter ranges in the disk and planetary mass for outward migration.

In this paper, we have discussed intrinsic physics of the outward migration and derived a general semi-analytical formula of the migration rate including outward migration.

The surface density of gas in the leading horseshoe-CPD region is higher than in the trailing horseshoe region, according to repeated mass loss from horseshoe flow to the planet during many-times horseshoe excursions. This azimuthal asymmetry causes positive corotation torque, resulting in outward migration of the planet. If the planetary gas accretion effect is neglected, this azimuthal asymmetry never appears and the radial asymmetry drives the conventional inward migration. Therefore, whether the migration is inward or outward is regulated by competition between the azimuthal asymmetry by the corotation torque and the radial asymmetry mostly due to Lindblad torque (Eqs. (36) and (37)).

We found that the condition for the outward migration is regulated mostly by the gap depth: i) The gap is deep enough to remain the dominance of horseshoe corotation torque over Lindblad torque, and ii) it is shallow enough that the planet accretes most of disk gas accretion to maintain the azimuthal horseshoe asymmetry. Based on the results of Pan et al. (2025), we found that the outward migration condition is simply given by

$$K'_{\text{acc}} \lesssim K' \lesssim K'_{\text{gap}}; \quad (46)$$

$$K'_{\text{acc}} = 0.03 h_{0.05}; \quad K'_{\text{gap}} = 50, \quad (47)$$

where K' is the gap depth parameter defined by $\Sigma_{\text{gap}}/\Sigma_0 = 1/(1 + K')$ and given by $K' = 1.28 \times 10^8 q^2 h_{0.05}^{-5} \alpha_3^{-1}$, $q = m_p/M_*$, $h_{0.05} = h/0.05$, and $\alpha_3 = \alpha/10^{-3}$. This condition covers broad parameter space. For given h and α , it extends to the planet mass range of $1.5 \times 10^{-5} h_{0.05}^3 \alpha_3^{1/2} \lesssim q \lesssim 6.3 \times 10^{-4} \times h_{0.05}^{5/2} \alpha_3^{1/2}$.

For smaller α , for example, $\alpha = 10^{-4}$, the range shifts to smaller values by a factor 3 from the above range. Once a core exceeds the critical core mass ($\sim 3 \times 10^{-5}$) to start gas accretion, the migration is outward until it reaches $0.2M_J$. Because the migration of the low-mass planet is fast (the gap is still shallow) and the fast migration is outward, the impact on planet formation may be more significant for smaller α .

We also found that the absolute value of the outward migration rate is similar to that of the inward migration rate that neglects the azimuthal asymmetry but takes account of global disk gas depletion due to the planetary gas accretion, although the migration direction is opposite. Interpolating the outward and inward migration parameter regimes, we derived the general semi-analytical migration formula in Section 3.3.

Using the formula, we calculated evolution of concurrent growth and migration of planets starting with masses $10 M_\oplus$ to demonstrate that the outward migration plays an important role for the mass and semimajor axis distribution of gas giants, particularly in disk outer regions where the gap is shallower. It would potentially reproduce the observed pile-up of exoplanetary gas giants beyond 1 au, and could give an insight into formation of HR 8799-like systems. Detailed planet population synthesis calculations for quantitative comparison with the observed data of exoplanets will be done in a separate paper.

ACKNOWLEDGMENTS

S.I. is supported by JSPS Kakenhi grant 21H04512 and 23H00143. Y.P.L. is supported in part by the Natural Science Foundation of China (grants 12373070, and 12192223), the Natural Science Foundation of Shanghai (grant NO. 23ZR1473700).

REFERENCES

- Ayliffe, B. A., & Bate, M. R. 2009, *MNRAS*, **393**, 49
- Chen, Y.-X., Zhang, X., Li, Y.-P., Li, H., & Lin, D. N. C. 2020, *ApJ*, **900**, 44
- Choksi, N., Chiang, E., Fung, J., & Zhu, Z. 2023, *MNRAS*, **525**, 2806
- Dempsey, A. M., Lee, W.-K., & Lithwick, Y. 2020, *ApJ*, **891**, 108
- Dempsey, A. M., Muñoz, D. J., & Lithwick, Y. 2021, *ApJL*, **918**, L36
- Duffell, P. C., Haiman, Z., MacFadyen, A. I., D’Orazio, D. J., & Farris, B. D. 2014, *ApJL*, **792**, L10
- Dürmann, C., & Kley, W. 2015, *A&A*, **574**, A52
- . 2017, *A&A*, **598**, A80
- Guo, K., Ogiwara, M., Ida, S., et al. 2025, *ApJ*, **983**, 56
- Ida, S., & Lin, D. N. C. 2010, *ApJ*, **719**, 810
- Ida, S., Lin, D. N. C., & Nagasawa, M. 2013, *ApJ*, **775**, 42
- Ida, S., Tanaka, H., Johansen, A., Kanagawa, K. D., & Tanigawa, T. 2018, *ApJ*, **864**, 77
- Kanagawa, K. D., Muto, T., Tanaka, H., et al. 2015a, *ApJL*, **806**, L15
- Kanagawa, K. D., Tanaka, H., Muto, T., Tanigawa, T., & Takeuchi, T. 2015b, *MNRAS*, **448**, 994
- Kanagawa, K. D., Tanaka, H., & Szuszkiewicz, E. 2018, *ApJ*, **861**, 140

- Kley, W., & Nelson, R. P. 2012, [ARA&A](#), **50**, 211
- Lambrechts, M., Lega, E., Nelson, R. P., Crida, A., & Morbidelli, A. 2019, [A&A](#), **630**, A82
- Laune, J., Li, R., & Lai, D. 2024, [ApJ](#), **975**, 296
- Lega, E., Benisty, M., Cridland, A., et al. 2024, [A&A](#), **690**, A183
- Li, Y.-P., Chen, Y.-X., & Lin, D. N. C. 2023, [MNRAS](#), **526**, 5346
- Li, Y.-P., Chen, Y.-X., & Lin, D. N. C. 2024, [ApJ](#), 971, 130
- Lin, D. N. C., Bodenheimer, P., & Richardson, D. C. 1996, [Nature](#), **380**, 606
- Lin, D. N. C., & Papaloizou, J. 1986, [ApJ](#), **309**, 846
- Lynden-Bell, D., & Pringle, J. E. 1974, [MNRAS](#), **168**, 603
- Maeda, N., Ohtsuki, K., Suetsugu, R., et al. 2024, [ApJ](#), **968**, 62
- Maeda, N., Ohtsuki, K., Tanigawa, T., Machida, M. N., & Suetsugu, R. 2022, [ApJ](#), **935**, 56
- Miyoshi, K., Takeuchi, T., Tanaka, H., & Ida, S. 1999, [ApJ](#), **516**, 451
- Pan, J.-P., Li, Y.-P., Chen, Y.-X., Ida, S., & Lin, D. N. C. 2025, [ApJ](#), in press
- Robert, C. M. T., Crida, A., Lega, E., Méheut, H., & Morbidelli, A. 2018, [A&A](#), **617**, A98
- Rosenthal, M., Chiang, E., Ginzburg, S., & Murray-Clay, R. 2020
- Rosenthal, M. M., Chiang, E. I., Ginzburg, S., & Murray-Clay, R. A. 2020, [MNRAS](#), **498**, 2054
- Tanaka, H., Murase, K., & Tanigawa, T. 2020, [ApJ](#), **891**, 143
- Tanaka, H., & Okada, K. 2024, [ApJ](#), **968**, 28
- Tanaka, H., Takeuchi, T., & Ward, W. R. 2002, [ApJ](#), **565**, 1257
- Tanigawa, T., & Tanaka, H. 2016, [ApJ](#), **823**, 48
- Tanigawa, T., & Watanabe, S.-i. 2002, [ApJ](#), **580**, 506
- Wafflard-Fernandez, G., & Lesur, G. 2025, [A&A](#), **696**, A8
- Wittenmyer, R. A., Wang, S., Horner, J., et al. 2020, [MNRAS](#), **492**, 377
- Wu, H., & Li, Y.-P. 2024, [Universe](#), **11**, 1